Arch Appl Mech (2015) 85:481–502
DOI 10.1007/s00419-014-0924-0

ORIGINAL

Panagiotis Koutsovasilis · Nicolas Driot · Daxining Lu · Bernhard Schweizer

Quantification of sub-synchronous vibrations for turbocharger rotors with full-floating ring bearings

Received: 22 April 2014 / Accepted: 23 September 2014 / Published online: 9 October 2014

Abstract The correct capture and understanding of the bearing- induced rotor vibrations is nowadays a rather compulsory task, which should accompany the modeling and simulation work flow of high-speed rotor systems, such as turbochargers. The oil-film concentrated in the rotor's journal bearings is the root cause of the system's occurring nonlinear effects known as sub-synchronous vibrations, the behavior of which depends on both the system's geometric and dynamic configuration. In this paper, a methodology is applied for the case of a turbocharger with full-floating ring bearings that allows the quantification of the sub-synchronous vibrations during run-up simulations. It is conducted by considering both the wheel shaft and shaft-bearing geometry as a set of input parameters, the variation of which contributes in quantifying their influence upon the sub-synchronous evolution with respect to amplitude and duration criteria. Motivated by linear multivariate regression algorithms and data mining techniques, i.e., correlation coefficients and global sensitivity methods, the influence of each design parameter on the sub-synchronous formation is analyzed. Furthermore, with the help of the non-supervised neural network methods, design configurations are indicated that could be set as a compromise in terms of feasibility and low-cost production.

Keywords Rotor dynamics · Oil-film bearings · Run-up simulations · Sub-synchronous vibrations · Shaft and Bearing design · Data mining

1 Introduction

The modeling and simulation work flow of turbocharger rotors is constantly becoming a demanding task. The implementation of the CO_2 regulations with respect to the automotive emission constitutes the application of

P. Koutsovasilis (✉) · N. Driot
Rotordynamics and Preventive Acoustics, Global Engineering Core Science,
BorgWarner Turbo Systems Engineering GmbH, Marnheimer Strasse 85/87,
67292 Kirchheimbolanden, Germany
E-mail: PKoutsovasilis@borgwarner.com

N. Driot
E-mail: ndriot@borgwarner.com

D. Lu · B. Schweizer
Strukturdynamik und Strukturüberwachnung, Technische Universität Darmstadt,
Otto-Berndt-Strasse 2, 64287 Darmstadt, Germany
E-mail: lu@sds.tu-darmstadt.de

B. Schweizer
E-mail: schweizer@sds.tu-darmstadt.de

turbocharger-equipped internal combustion engines rather mandatory. Engine downsizing is the first conceptual step to be conducted, but should be accompanied by extra implementation measures in order to keep up with the also increasing engine performance characteristics. In this regard, the conventional turbocharger virtual prototyping methodology should be extended, thus accounting for the new set of downsizing-induced boundary conditions, which affect both the system's efficiency and life time span. On one hand, the known rotor vibration effects should be better captured and on the other hand the associated noise phenomena ought to be better handled, since the downsized motors have to also operate on lower decibel scales. Therefore, the correct capture and understanding of the oil-film bearing-induced sub-synchronous vibrations is nowadays a rather compulsory task, which should accompany the modeling and simulation work flow of turbochargers.

On the basis of the aforesaid, the paper is organized as follows: In the second chapter, a brief description is given with respect to the modeling procedure of the turbocharger rotor with full-floating ring bearings. The main features of the run-up simulation are presented, which should constitute the kernel for the presented methodology. The third chapter comprises of the detailed allocation of the system's response space, i.e., output data, based on which the rotor-bearing configurations will be evaluated. The fourth chapter includes the detailed description for the proposed methodology, which is divided into two major categories, i.e., the shaft-bearing position design and the shaft-bearing dimension design. For each of these categories, the associated space of input data is outlined, which defines the basis for a parameter variation study. The fifth chapter copes with an extended investigation and results' illustration of the aforementioned parameter variation study with the help of multivariate regression algorithms as well as data mining techniques in order to quantify the influence of each design parameter upon the sub-synchronous formation. Finally, the application of an unsupervised neural network methodology known as self-organizing maps (SOM) is included, which allows the indication of design configurations that could be set as a compromise in terms of feasibility and low-cost production. The conclusions are included in the last chapter.

2 Turbocharger run-up simulation: rotor-bearing model

As depicted in Fig. 1, the turbocharger rotor-bearing model with semi- or full-floating ring bearings is defined as an assembly of rigid (e. g., bearings and wheels) and flexible bodies (e.g., shaft), which interact with each other due to the presence of joints and force elements (e.g., bearing forces). Based on the floating frame of reference formulation [37,38], the motion equations of such constrained mechanical multi-body systems (MBS) are given by second order, index-3 differential-algebraic equations (DAE) [1,2,5,13], i.e.,

$$\mathbf{M}(\mathbf{q})\ddot{\mathbf{q}}(t) = \mathbf{h}(\mathbf{q}, \dot{\mathbf{q}}, t) - \mathbf{G}^T(\mathbf{q}, t)\boldsymbol{\lambda} \tag{1}$$

$$\mathbf{0} = \mathbf{g}(\mathbf{q}, t) \tag{2}$$

Here, $\mathbf{q}^T \in \mathbb{R}^{n\times 1}$, $n \in \mathbb{N}^*$ represents the set of generalized coordinates, $\mathbf{M} \in \mathbb{R}^{n\times n}$ the symmetric mass matrix and $\mathbf{h}(\mathbf{q}, \dot{\mathbf{q}}, t) \in \mathbb{R}^{n\times 1}$ the vector containing all applied and velocity-dependent inertia forces. The generalized constraint forces $-\mathbf{G}^T(\mathbf{q}, t)\boldsymbol{\lambda} \in \mathbb{R}^{n\times 1}$ are defined by the associated Jacobian matrix $\mathbf{G} := (\partial\mathbf{g}/\partial\mathbf{q})(\mathbf{q}, t)$ and the Lagrange multipliers $\boldsymbol{\lambda} \in \mathbb{R}^{n_c}$ satisfying the existing n_c constraints.

In order to account for the drift-off occurrence associated with the additional hidden constraints on the state variables $\mathbf{q}$ and $\boldsymbol{\lambda}$ [1,2,5,24], the Gear–Gupta–Leimkuhler—or stabilized index-2- formulation [15] is adopted throughout the subsequent rotor dynamics calculations and solved based on a backward differentiation formula (BDF) solver [5]:

$$\dot{\mathbf{q}}(t) = \mathbf{u} - \mathbf{G}^T(\mathbf{q}, t)\boldsymbol{\mu} \tag{3}$$

$$\mathbf{M}(\mathbf{q})\dot{\mathbf{u}}(t) = \mathbf{h}(\mathbf{q}, \mathbf{u}, t) - \mathbf{G}^T(\mathbf{q}, t)\boldsymbol{\lambda} \tag{4}$$

$$\mathbf{0} = \mathbf{g}(\mathbf{q}, t) \tag{5}$$

$$\mathbf{0} = \mathbf{G}(\mathbf{q}, t)\mathbf{u} + \partial\mathbf{g}/\partial t(\mathbf{q}, t) \tag{6}$$

$$\boldsymbol{\mu}(t) \in \mathbb{R}^{n_c} \ : \ \text{auxiliary variable}$$

The wheels and journal bearings are introduced into the multi-body model (3)–(6) as rigid bodies, thus containing the information only w.r.t. the mass, center of mass and the associated moments of inertia (polar and diametrical).

On the contrary, the shaft is modeled as a flexible body, which is discretized with linear finite elements (FE) and incorporated in (3)–(6) by the application of the conventional model order reduction (MOR) scheme

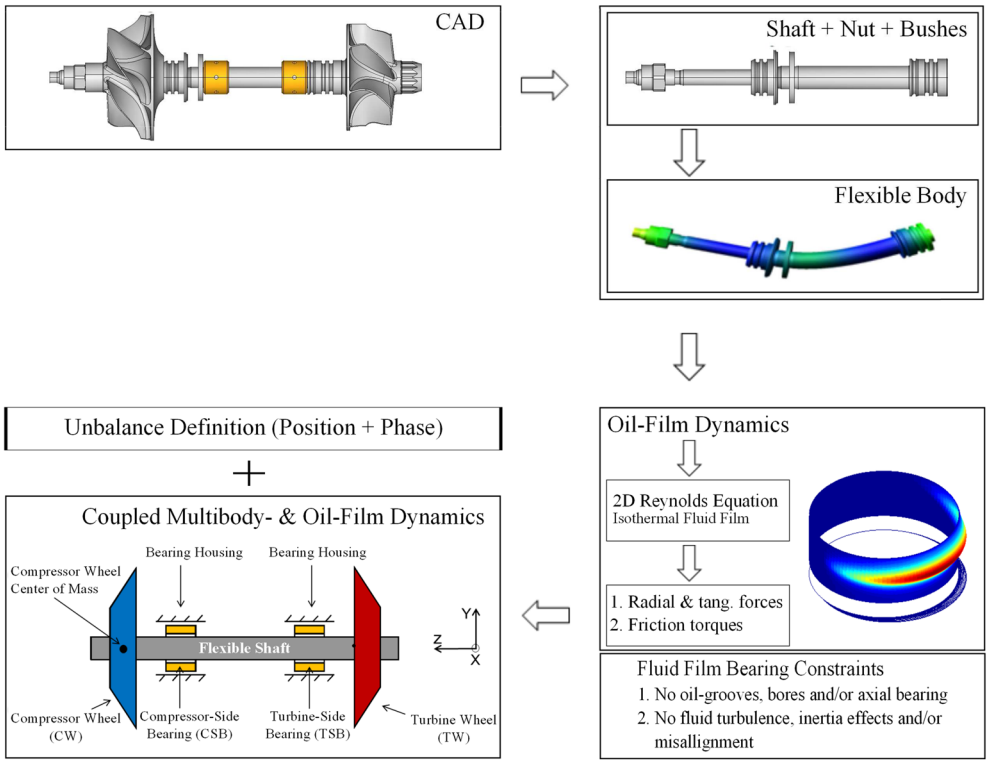

Fig. 1 Turbocharher rotordynamics—modeling procedure

known as component mode synthesis (CMS) [4,7,8,22,23,25]. The frequency threshold to be defined during the MOR should appoint to a reduced model, which incorporated into the MBS (3)–(6) captures perfectly the system's natural gyroscopic frequencies up to the predefined rotor speed limit [4,34,35]. In this regard, it is ascertained that the sub-synchronous -also known as oil-whirl/whip- excited gyroscopic modes occur at the correct frequency range [33–35]. The root cause of the aforementioned sub-synchronous vibrations is the oil-film concentrated in the rotor's journal bearings, which in case of turbocharger rotors with full-floating ring bearings drives the system to exhibit the following basic sub-synchronous responses [4,6,14,29,34,36,40]:

- 1st sub-synchronous (Sub_1) with the oil-whirl/whip of the inner oil-film exciting the gyroscopic conical forward mode,
- 2nd sub-synchronous (Sub_2) with the oil-whirl/whip of the inner oil-film exciting the gyroscopic translational forward mode,
- 3rd sub-synchronous (Sub_3) with the oil-whirl/whip of the outer oil-film exciting the gyroscopic conical forward mode.

Within the framework of this paper, the oil-flow and pressure generation in both the inner and outer clearanced bearings is calculated by solving the Reynolds equation [4,6,34,39] under the restrictions quoted in Fig. 1 (for details see Appendix A). The fluid-film forces along with the friction torques are incorporated into the MBS (3)–(6) for conducting the subsequent rotor dynamic simulations via lookup tables [33–36]. The rotor is driven by a prescribed motion applied at the turbine wheel center of mass (Fig. 1).

Finally, the information w.r.t. rotor imbalance is represented by point masses, which are fixed at the compressor and the turbine wheel at specific positions, thus allowing to account for in- and out-of-phase imbalance definitions.

3 Turbocharger run-up simulation: configuration of the response space

The variety of parameters that influence the rotor dynamics of either simple Jeffcott or complex turbocharger rotors has been extensively investigated in the literature during the past years. In particular, the influence of a

Table 1 Configuration of the response space

Variable	Description	Unit
CW_{rel}	Radial displacement of the CW center of mass at maximum RPM	(mm)
CSB_{e_o}	CSB outer eccentricity at maximum RPM	(–)
CSB_{e_i}	CSB inner eccentricity at maximum RPM	(–)
TSB_{e_o}	TSB outer eccentricity at maximum RPM	(–)
TSB_{e_i}	TSB inner eccentricity at maximum RPM	(–)
Sub_1^A	Begin of the 1st sub-synchronous mode	(1/min)
Sub_1^E	End of the 1st sub-synchronous mode	(1/min)
Sub_2^A	Begin of the 2nd sub-synchronous mode	(1/min)
Sub_2^E	End of the 2nd sub-synchronous mode	(1/min)
Sub_3^A	Begin of the 3rd sub-synchronous mode	(1/min)
Sub_1^{amp}	Max. amplitude of the 1st sub-synchronous mode	(mm)
Sub_2^{amp}	Max. amplitude of the 2nd sub-synchronous mode	(mm)
Sub_3^{amp}	Max. amplitude of the 3rd sub-synchronous mode	(mm)

CSB compressor side bearing , *TSB* turbine side bearing, *CW* compressor wheel—radial displacement as defined in Fig. 1, e_i inner eccentricity, e_o outer eccentricity

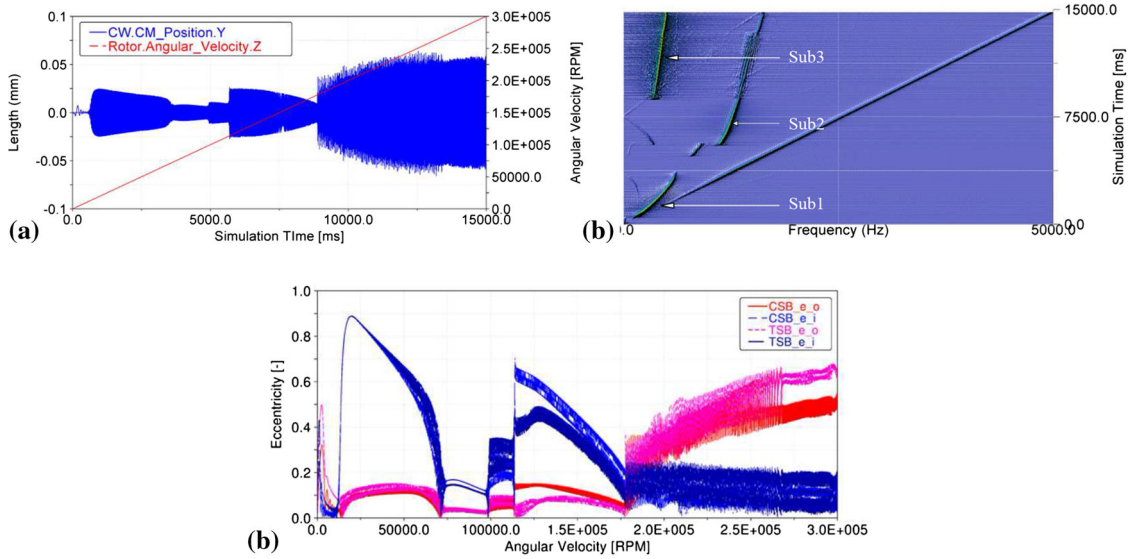

Fig. 2 Run-up simulation of a rotor with full-floating bearings: **a** radial displacement of the compressor wheel's center of mass (CW.CM), **b** associated waterfall diagram indicating the sub-synchronous responses, **c** inner e_i & outer e_o eccentricities for the compressor side (CSB) and turbine side (TSB) bearing

rotor's bearing parameters upon several responses, e.g., friction loss and pressure forces, boundary oil-flow, sub-synchronous has been shown in [14,18,26,29–31,40] in form of characteristic curves and non-dimensional parameter ratios. The impact of external/base excitation and geometric uncertainties was demonstrated for a jeffcott rotor study in [9–11], whereas an extended survey on the bifurcation evolution of several jeffcott and turbocharger rotor model configurations was the core research in [3,34,35]. All above contributes in acquiring empirical statements or non-dimensional quantities, e.g., Sommerfeld numbers, which ultimately deliver a qualitative information for the properties that influence the system's response.

Here, a different approach is undertaken in an effort to account for both qualitative as well as quantitative information w.r.t. the influence of the investigated parameters on specified system responses, but also among the responses themselves. In this regard, the definition of the associated response configuration space is conducted as given in Table 1. The data should be considered as supplementary information to the conventional run-up simulation results shown in Fig. 2.

In the special case of turbochargers with full-floating ring bearings, there exist two major rotor instability bottlenecks, i.e., the second (Sub_2) and the third (Sub_3) sub-synchronous mode. As introduced in [3,33–35], several sub-synchronous sequences are often observed in turbocharger run-ups, the occurrence of which cannot be a priori predicted. Therefore, in Table 1, the information w.r.t. to the beginning and ending of each

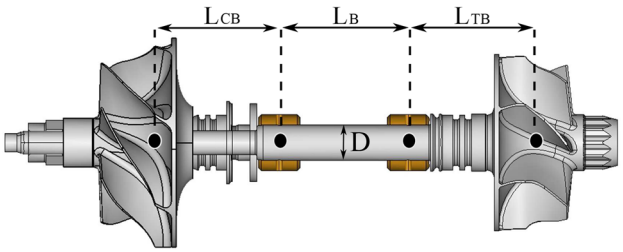

Fig. 3 Study I: Parameter definition

Table 2 Study I: Shaft-bearing position design—DoE parameter space based upon the reference configuration

Variable	Reference (%)	Min (%)	Mean (%)	Max (%)	Range (%)
D	100	86.6	93.3	100	13.33
L_B	100	75.3	96.5	105	29.7
L_{CB}	100	73.68	100.6	105	31.3
L_{TB}	100	90	99	110	20

The above parameters are depicted in Fig. 3 and normalized on the basis of a 100% reference configuration
A total of 20 configurations are computed (DoE-dimension of Study I)
D: Diameter of the shaft part between the two bearings, L_B: distance between the center of masses of the two bearings, L_{CB}: center of mass distance between the compressor wheel and the compressor side bearing, L_{TB}: center of mass distance between the turbine wheel and the turbine side bearing

sub-synchronous is included as a mandatory response to be evaluated during each run-up simulation. It is not only the sub-synchronous amplitude that has to be captured (Table 1), but the duration of each of the aforementioned vibrations (in RPM), since for example a Sub_3 optimized turbocharger might suffer from extended Sub_2-induced constant tone issues, etc. Furthermore, the inner and outer eccentricity information at maximum RPM for both the compressor and turbine side bearing is assessed in order to acquire the information to which of the oil-film becomes unstable based on the associated turbocharger rotor configuration. Finally, the radial displacement of the compressor wheels center of mass at maximum RPM is included leading to a total of 13 scalar quantities defining the configuration space of responses. The reason for considering the latter is twofold: Firstly, it is accustomed for this information to be included as an output in turbocharger run-ups due to correlation grounds w.r.t. to measurements, and secondly, because this output is composed based on all signals (synchronous and sub-synchronous), it enables the correlation of the observed compressor wheel's radial displacement and the investigated sub-synchronous responses.

4 Turbocharger run-up simulation: parameter variation & boundary conditions

4.1 Study I: Shaft-bearing position design

The aim of the first study is to account for the influence of a rotor's macro design geometry upon the set of responses defined in Table 1. The macro-geometry regards the shaft-bearing position design as depicted in Fig. 3.

The interspace between the bearing sleeve and the right-hand-side shaft end is parameterized by means of defining three distance quantities L_{CB}, L_B and L_{TB} (Fig. 3). These quantities are set as independent parameters for a variation study, which is defined in terms of a Design of Experiment (DoE) [27] as given in Table 2. Furthermore, the diameter D of the shaft part located between the two bearings (Fig. 3) is set as an extra DoE parameter. Herewith, various rotor assemblies are generated, all of which have both different shaft diameter and total length, which directly indicates that the flexible shaft-modeling process described in Sect. 2 and Fig. 1 should be repeated according to the predefined dimension of the DoE (Table 2). The rest of rotor assembly design parameters are left intact.

Study I is applied for a rotor-bearing model with its basic configuration being listed in Table 3. It copes with a small-sized high-speed turbocharger rotor with full-floating ring bearings. The size as well as the maximum operating speed (3×10^5 RPM) indicates that the aforementioned vibration effects (Sub_2 & Sub_3) are not to

Table 3 Study I: Shaft-bearing position design—basic rotor- assembly information

Design information of rotor assembly	Approximate value (≈)	Unit
Total rotor assembly mass	70	(g)
Total rotor assembly length	100	(mm)
Bearing ring inner & outer diameter	6 & 9.5	(mm)
Bearing ring inner & outer width	3.5 & 6	(mm)
Reference bearing shaft diameter D	6	(mm)
Reference length $L = L_{\mathrm{CB}} + L_B + L_{\mathrm{TB}}$	65	(mm)
Unbalance at compressor & turbine wheel	2×0.03@0 °C & 2×0.03@0 °C	(gmm)
Dynamic oil viscosity at 20 °C	0.16	($\mathrm{Ns/m^2}$)
Oil supply temperature	150	(°)
Rotor speed range (ramp acceleration)	$[0, \quad 3] \cdot 10^5$	(1/min)

Table 4 Study II: Shaft-bearing dimension design—DoE parameter space based upon the reference configuration

Variable	Reference (%)	Min (%)	Mean (%)	Max (%)	Range (%)
D_1	100	91.6	92.8	100	8.33
D_2	100	91.6	98.8	105	8.33
CSB_{ψ_o}	100	85.7	94.2	100	14.3
CSB_{ψ_i}	100	81.3	97.5	125	43.8
CSB_{W_o}	100	100	123.3	130	30
CSB_{W_i}	100	77.8	97.6	100	22
CSB_{ψ_o}	100	100	109	116	16
CSB_{ψ_i}	100	59	78.6	100	40.9
CSB_{W_o}	100	89.1	112.3	116	26.8
CSB_{W_i}	100	92.6	112	128.6	35.7
T_{sup}	100	100	126.9	166.7	66.7

The above parameters are normalized on the basis of a 100 % reference configuration
A total of 45 configurations are computed (DoE-dimension of Study II)
CSB compressor side bearing , *TSB* turbine side bearing, D_1 CSB shaft diameter, D_2 TSB shaft diameter, ψ_i inner clearance, ψ_o: outer clearance, W_i inner width, W_o outer width, T_{sup} oil supply temperature with $T_{\mathrm{sup}}^{\mathrm{min}} = 90\,^{\circ}\mathrm{C}$ & $T_{\mathrm{sup}}^{\mathrm{max}} = 150\,^{\circ}\mathrm{C}$

be avoidable. While Sub_2 could be listed under comfort-issue problems, Sub_3 with extended amplitudes might lead to rotor destruction.

It should be mentioned that the methodology applied for Study I and the subsequent Study II is not restricted on how to vary the investigated parameters. Here, it is conducted by means of DoE, but the application of multivariate analysis algorithms for defining the parameter space with the help of sampling methods, e.g., random, Monte Carlo and Latin Hypercube is not excluded [17,26].

4.2 Study II: Shaft-bearing dimension design

Here, the parameters regarded for variation via multiple run-up simulations are those directly involved in the Reynolds equation for describing the fluid-film dynamics. Therefore, the compressor and turbine side bearing's clearance and width for both the inner and outer oil-films are taken into consideration. Additionally, Study II is extended by accounting as independent parameter the shaft diameter along the rotor length $L = L_{\mathrm{CB}} + L_B + L_{\mathrm{TB}}$ (Fig. 3), but separated into two parts: D_1 denoting the compressor side bearing shaft part of L and D_2 analogously defined for the turbine side bearing shaft part of L. Finally, contrary to Study I, the oil supply temperature is also set as a parameter to be varied, but only for the case of coping with either a cold ($T_{\mathrm{sup}}^{\mathrm{min}} = 90\,^{\circ}\mathrm{C}$) or a warm ($T_{\mathrm{sup}}^{\mathrm{max}} = 150\,^{\circ}\mathrm{C}$) boundary condition. All above 11 parameters are listed in Table 4, the combination of which results in a total of 45 different rotor- assembly configurations.

The parameter influence of both studies I and II is separately assessed in the following Sect. 5 in terms of data mining analysis. Aim is firstly to provide a general suggestion scheme w.r.t. to the macro-geometry of the rotor-bearing assembly (Study I). Thereafter, on the basis of a quasi-optimized macro-geometry the additional information w.r.t. the parameters influencing the bearing dynamics should be indicated, thus leading to an overall optimum rotor assembly design under the frame conditions defined by the set of responses (Table 1).

5 Turbocharger run-up simulation: data mining analysis

5.1 Study I: Shaft-bearing position design

Data mining analysis [19,27] copes with producing a low-dimensional space of multivariate samples in terms of quantitative measures for characterizing the dependencies among the samples. For that purpose, the Pearson correlation coefficient [19,26,27,32]

$$r(\mathbf{T},\mathbf{T}) = \frac{\sum_{i\neq j}^{n}\left(t_{ij}-\mu_{\mathbf{T}}\right)\left(t_{ij}-\mu_{\mathbf{T}}\right)}{\sqrt{\sum_{i\neq j}^{n}\left(t_{ij}-\mu_{\mathbf{T}}\right)^2}\sqrt{\sum_{i\neq j}^{n}\left(t_{ij}-\mu_{\mathbf{T}}\right)^2}}$$
$$\mu_{\mathbf{T}}\ :\ \text{sample means},\quad t_{ij}\ :\ ij\text{-th element of}\ \ \mathbf{T}$$
$$\mathbf{T}=\{\mathbf{R}\ ,\ \mathbf{V}\},\quad \mathbf{R}:\ \text{matrix of Responses},\quad \mathbf{V}:\ \text{matrix of Variables} \tag{7}$$

is utilized with $\mathbf{T}$ being the data matrix, which collects the information of variables or responses stored both in a columnwise format. The Pearson coefficient varies between -1 and 1, with 1 denoting a perfect increasing linear correlation between the compared data and -1 an equivalent perfect anti-correlation. The values in-between serve as indication factors w.r.t. the linear dependence degree of the compared data.

Figure 4 gathers the Pearson correlation information w.r.t. Study I, all of which is summarized in the following Table 5.

In contrast to the Pearson coefficient, the Coefficient of Importance (CoI) [12,32] indicates the possible multivariate dependencies of a group of input parameters (for details see Appendix B.1). CoI indicates the influence of a single input variable among the complete set of input variables upon a chosen response. Figure 5 gathers the CoI results for the current Study I, which can be interpreted as follows:

– rowwise with each "FullR^2" indicating the approximate total amount of variance for the associated response due to all variables. This value is decomposed into each variable-induced variance, while simultaneously considering the variance of the rest of the variables (Table 2)

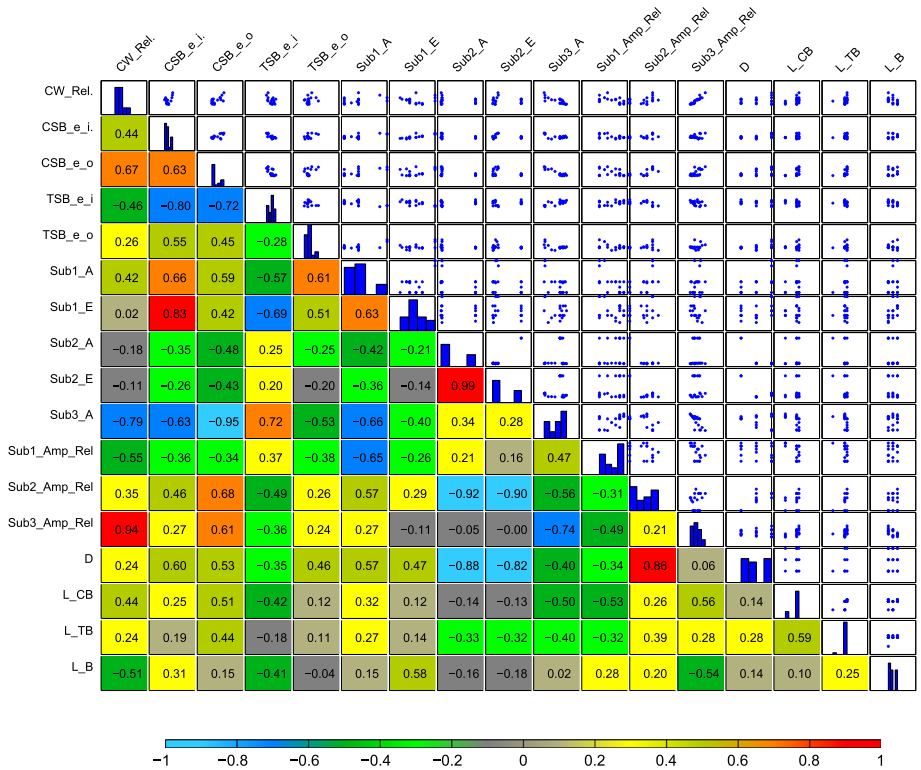

Fig. 4 Study I: Pearson correlation matrix

Table 5 Study I: Shaft-bearing position design—major input & output dependencies

Parameter	Influence on inner & outer oil-film (e_i & e_o for both CSB & TSB)	Influence on $\text{Sub}_{1,2,3}^{\text{amp}}$- & duration
D	A flexible shaft with small diameter operates overall positive for the CSB, but negative for the TSB inner oil-film. Herewith, a possibility of a shaft concept with asymmetrical diameter could be favored	A flexible shaft with small diameter operates positively for $\text{Sub}_3^{\text{amp}}$, but results with elongated Sub_2 (constant tone) and larger $\text{Sub}_1^{\text{amp}}$
L_B	A small L_B acts positive for the CSB and negative for the TSB inner oil-film	A small L_B acts negatively for $\text{Sub}_3^{\text{amp}}$
L_{CB}	A small L_{CB} acts positive for the outer CSB oil-film, but negative for the inner TSB oil-film	A small L_{CB} acts positive w.r.t. $\text{Sub}_3^{\text{amp}}$, but negative w.r.t. $\text{Sub}_1^{\text{amp}}$, although both are conical modes
L_{TB}	A small L_{TB} acts positive for the outer CSB oil-film	A small L_{TB} acts positive w.r.t. $\text{Sub}_{2,3}^{\text{amp}}$, but negative w.r.t. $\text{Sub}_1^{\text{amp}}$ (negligible correlations)

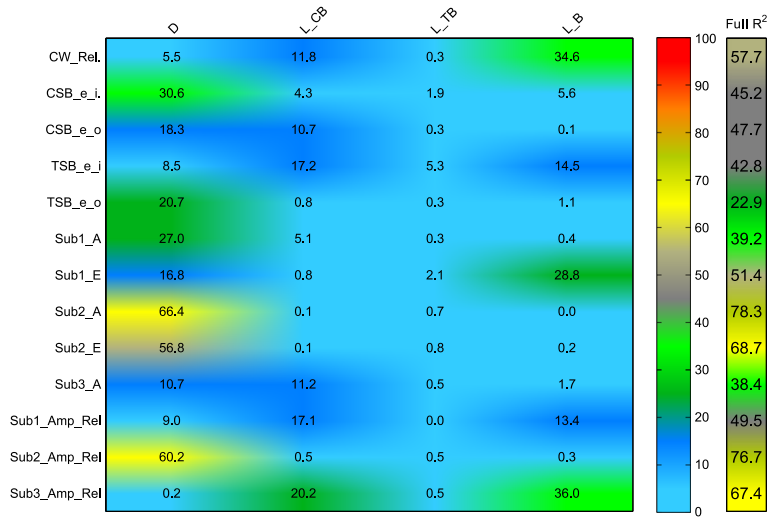

Fig. 5 Study I: coefficient of importance (CoI)

– columnwise depicting the associated variable's interaction with the investigated set of responses.

Figure 5 clearly depicts that the shaft diameter D interacts with almost the whole response space, whereas L_{TB} shows no interaction at all. Extended interaction dependencies of all input data and the sub-synchronous responses are given in details in Appendix B.2 with the help of Response Surface Methodology [28].

The aforementioned conclusion is confirmed by the application of sensitivity analysis. It is computed by performing linear regression analysis on the matrix of the responses **R** using the matrix of variables **V**, and then, a standard principal component analysis (PCA) is conducted on the approximate matrix obtained by multidimensional regression [12,16,32]. The computed regression coefficients are used as ranking variables for the global sensitivity of the Study I parameters, i.e., pinpointing the variables (Table 2) that have the most influence upon the global set of responses as defined in Table 1. The results are depicted in Fig. 6. For details w.r.t. to the sensitivity analysis of the parameters upon each individual response of the associated response configuration space, see Appendix B.3.

Both the sensitivity analysis results (Fig. 6) as well as the CoI coefficient (Fig. 5) quantify the shaft diameter D being the most influential input variable (39% influence) upon the global set of responses (Table 1). On the other hand, the role of L_{TB} is subordinate (10 % influence), whereas L_{CB} and L_B are rated as equally important (26 and 25 % influence, respectively). The latter though exhibit controversial properties w.r.t. the amplitude of Sub_3 and the CSB and TSB outer oil-film (Table 5). Therefore, L_B and L_{CB} should be designed so as to neutralize the inherited opposite effects between the CSB and TSB oil-films, and Sub_3 itself.

On the basis of the aforesaid, the optimized shaft-bearing position design is proposed in Table 6.

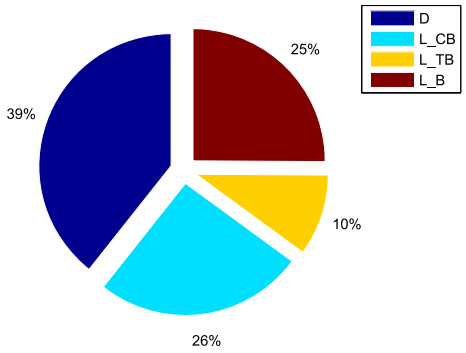

Fig. 6 Study I: sensitivity analysis

Table 6 Study I: Shaft-bearing position design—optimized design based on the 100 % reference configuration

Variable	Design suggestion based on the reference configuration
D	Utilization of an asymmetric shaft design ($D_{\mathrm{CSB}} < D_{\mathrm{CSB}}^{\mathrm{Ref}} < D_{\mathrm{TSB}} = D_{\mathrm{TSB}}^{\mathrm{Ref}}$)
L_B	Increase the dimension as much as possible ($L_B > L_B^{\mathrm{Ref}}$)
L_{CB}	Decrease the dimension allowed by the rotor assembly constraints ($L_{\mathrm{CB}} < L_{\mathrm{CB}}^{\mathrm{Ref}}$)
L_{TB}	Either decrease or leave unchanged ($L_{\mathrm{TB}} \leq L_{\mathrm{TB}}^{\mathrm{Ref}}$)

Table 7 Study II: Shaft-bearing dimension design–major input & output dependencies

Parameter	Influence on inner & outer oil-film (e_i & e_o for both CSB & TSB)	Influence on $\mathrm{Sub}_{1,2,3}^{\mathrm{amp}}$- & duration
D_1	The smaller the CSB shaft part diameter is, the better the outer oil-film response is	The smaller the CSB shaft part diameter is, the better $\mathrm{Sub}_{1,2,3}^{\mathrm{amp}}$ is
D_2	A large TSB shaft part diameter acts positive for both outer oil-films	A large TSB shaft part diameter acts positive for $\mathrm{Sub}_3^{\mathrm{amp}}$
ψ_o	Large ψ_o values result in very unstable outer oil-films	Large ψ_o values cause large $\mathrm{Sub}_3^{\mathrm{amp}}$ and contribute in all $\mathrm{Sub}_{1,2,3}$ occurring earlier in the RPM range
W_o	Large W_o values contribute in stabilizing the outer oil-films	Large W_o values contribute in stabilizing $\mathrm{Sub}_3^{\mathrm{amp}}$, but induce simultaneously larger $\mathrm{Sub}_{1,2}^{\mathrm{amp}}$ that occur earlier in the RPM range
ψ_i	Only TSB_{ψ_i} shows positive correlation to a system response, i.e., the TSB inner oil-film	–
W_i	A large TSB_{W_i} correlates to a destabilized inner oil- and a stabilized outer oil-film	A large TSB_{W_i} correlates to larger $\mathrm{Sub}_3^{\mathrm{amp}}$ that occurs earlier in the RPM range
T_{sup}	Large oil supply temperatures have a direct destabilizing effect for both inner oil-films	Large oil supply temperatures cause $\mathrm{Sub}_{1,2}^{\mathrm{amp}}$ to occur earlier in the RPM range (small correlation strength)

5.2 Study II: Shaft-bearing dimension design

The data mining procedure occurs analogously for Study II. The Pearson correlation results are depicted in Fig. 7 with the major contributions w.r.t. linear analogies among input and outputs being gathered in Table 7. As in Study I, here also the advantage of utilizing an asymmetric diameter for the CSB- and the TSB shaft part is clearly noted (Table 7). It is observed that several of the design parameters exhibit positive behavior w.r.t. to a specific response, e.g., large W_o induces smaller $\mathrm{Sub}_3^{\mathrm{amp}}$, but simultaneously cause problems w.r.t. to other responses, e.g., large W_o causes larger $\mathrm{Sub}_{1,2}^{\mathrm{amp}}$.

The importance of each parameter upon the global set of responses is assessed by applying the sensitivity analysis, the results of which are depicted in Fig. 8. Here, almost 40 % of the system's global response is controlled by the design of the outer clearances (CSB_{ψ_o} & TSB_{ψ_o}), thus directly indicating the compulsory design modification. The suggestion of utilizing smaller outer clearances in case of coping with Sub_3 issues is an experience-based solution, which in the framework of the current analysis is in addition quantified (≈40 %).

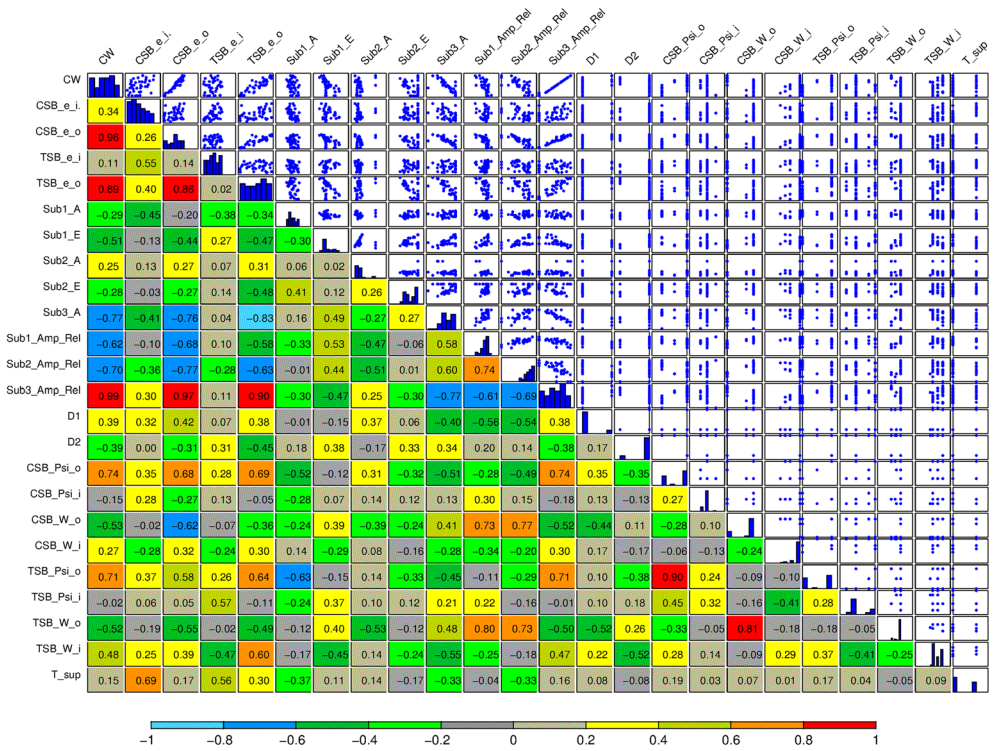

Fig. 7 Micro-geometry study—Pearson correlation matrix

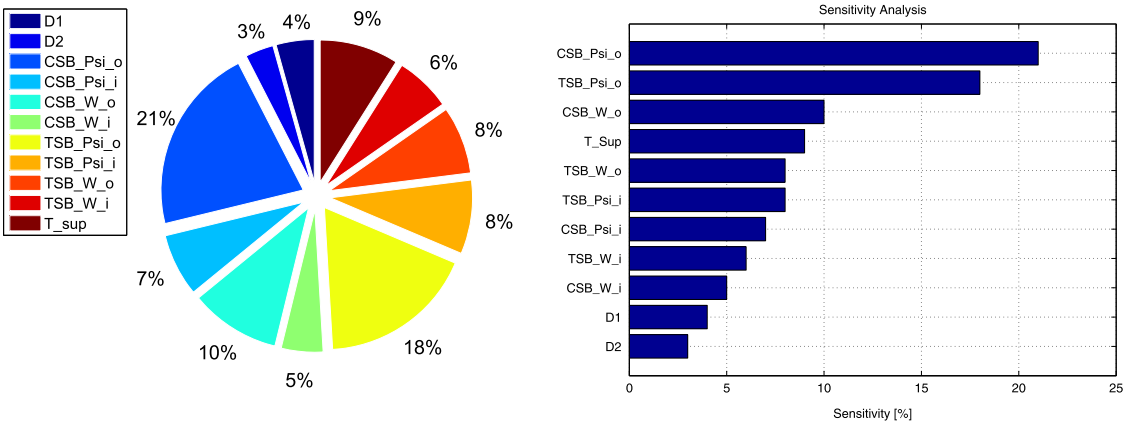

Fig. 8 Micro-geometry study—sensitivity analysis

The bearings' outer width is further listed as important factors, which along with the outer clearances contribute in influencing over 55 % of the system's global response as defined in Table 1. Of course, as already noted in Table 7, an enlargement of the bearing outer width although Sub_3-beneficial, it acts contra-productive w.r.t. to constant tone problems (Sub_2).

An interesting aspect regards the oil supply temperature T_{sup}. It is ranked as the fourth most important parameter with its tendency w.r.t. correlation being noted in Table 7. The oil supply temperature is directly involved with both the properties of the oil (viscosity) and the interacted materials parts (shaft, bearing, housing) affecting directly the associated bearing speed. For further details w.r.t. to the sensitivity analysis of the parameters upon each individual response of the associated response configuration space, see Appendix C.1.

Since, a turbocharger rotor has to perform equally well under cold and warm conditions (cold-start or friction loss problems), the presented results are extended by applying the Self-Organizing Maps (SOM) methodology

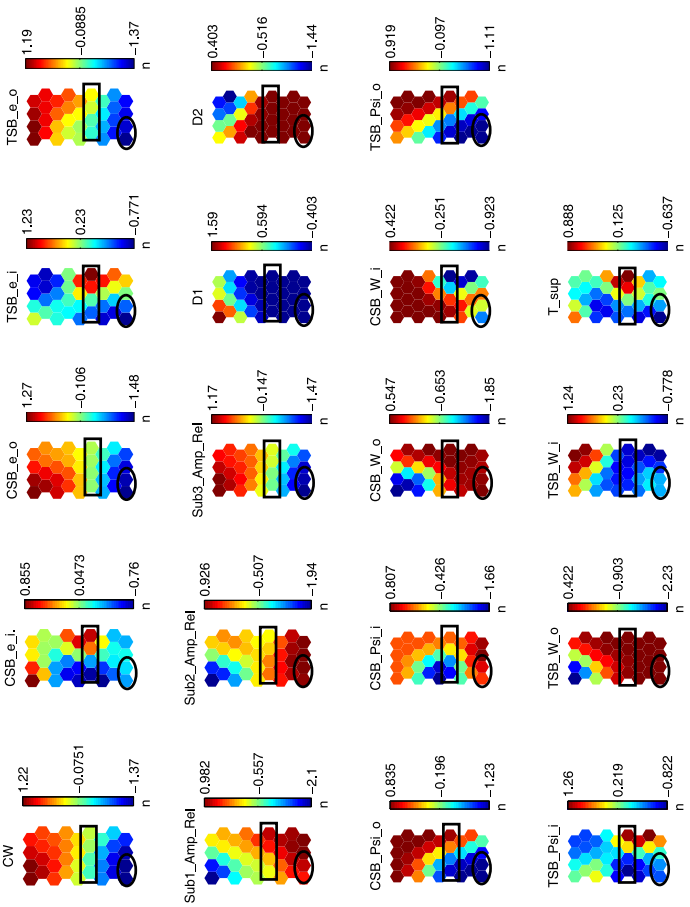

Fig. 9 SOM analysis—Study II—normalized responses

[20,21] in order to account for a feasible rotor assembly design that would hold on to the addressed cold and warm prerequisites.

Figure 9 gathers the SOM results, based on which four major conclusions are drawn for the specific rotor assembly:

1. The similarity in the SOM pattern for $\mathrm{Sub}_1^{\mathrm{amp}}$ and $\mathrm{Sub}_2^{\mathrm{amp}}$ indicates a quasi-linear behavior between these two responses, i.e., their evolution is linearly inter-dependent. Additionally, the reversed similarity among $\mathrm{Sub}_{1,2}^{\mathrm{amp}}$ and $\mathrm{Sub}_3^{\mathrm{amp}}$ denotes the anti-linear behavior of these responses, i.e., it is impossible to reach to a simultaneous optimal solution w.r.t. all $\mathrm{Sub}_{1,2,3}^{\mathrm{amp}}$.
2. The CW response is highly dominated by $\mathrm{Sub}_3^{\mathrm{amp}}$, which in turn possesses a similar pattern w.r.t. to both outer eccentricities, thus indicating a linear analogy (that explains the ≈40 % influence on the system's global response).
3. The similarity in the SOM pattern of both bearing's outer widths (CSB_{W_o} and TSB_{W_o}) w.r.t. $\mathrm{Sub}_{1,2}^{\mathrm{amp}}$ and simultaneously the reversed pattern of the same input parameters w.r.t. both the outer oil-films (CSB_{e_o} and TSB_{e_o}). This fact exhibits the experienced-based conclusion of not being able to optimize all sub-synchronous responses for the case of turbocharger rotors with full-floating bearings.
4. The positive effect of utilizing a non-symmetric shaft diameter for the compressor and turbine side bearing. Besides the associated D_1 and D_2 dependencies noted in Table 7, a shaft with higher elasticity compared with the standards is insinuated, the positive properties of which w.r.t. bifurcation sequences is investigated in [3].

Furthermore, SOM is utilized for indicating a best-case scenario (elliptical selected cells in Fig. 9), but more importantly a compromise scenario (rectangular selected cells in Fig. 9) that holds for the whole oil supply temperature range (cold and warm condition) as well as for the complete min–max inner and outer

Table 8 Study II: Shaft-bearing dimension design—Optimized design based on the 100 % reference configuration

Parameter	Rotor assembly	
	Best Sub_3 configuration	Compromise $\text{Sub}_{1,2,3}$ configuration
D_1 & D_2	↘ & =	↘ & =
CSB_{ψ_o} & TSB_{ψ_o}	↘ & ↘	= & =
CSB_{ψ_i} & TSB_{ψ_i}	= & =	= & ↗
CSB_{W_o} & TSB_{W_o}	↗ & ↗	↗ & ↗
CSB_{W_i} & TSB_{W_i}	= & ↘	↘ & ↘

"↘" "↗" and "=" indicates parameters with dimension smaller, larger and equal than the associated parameter of the reference configuration rotor assembly, respectively

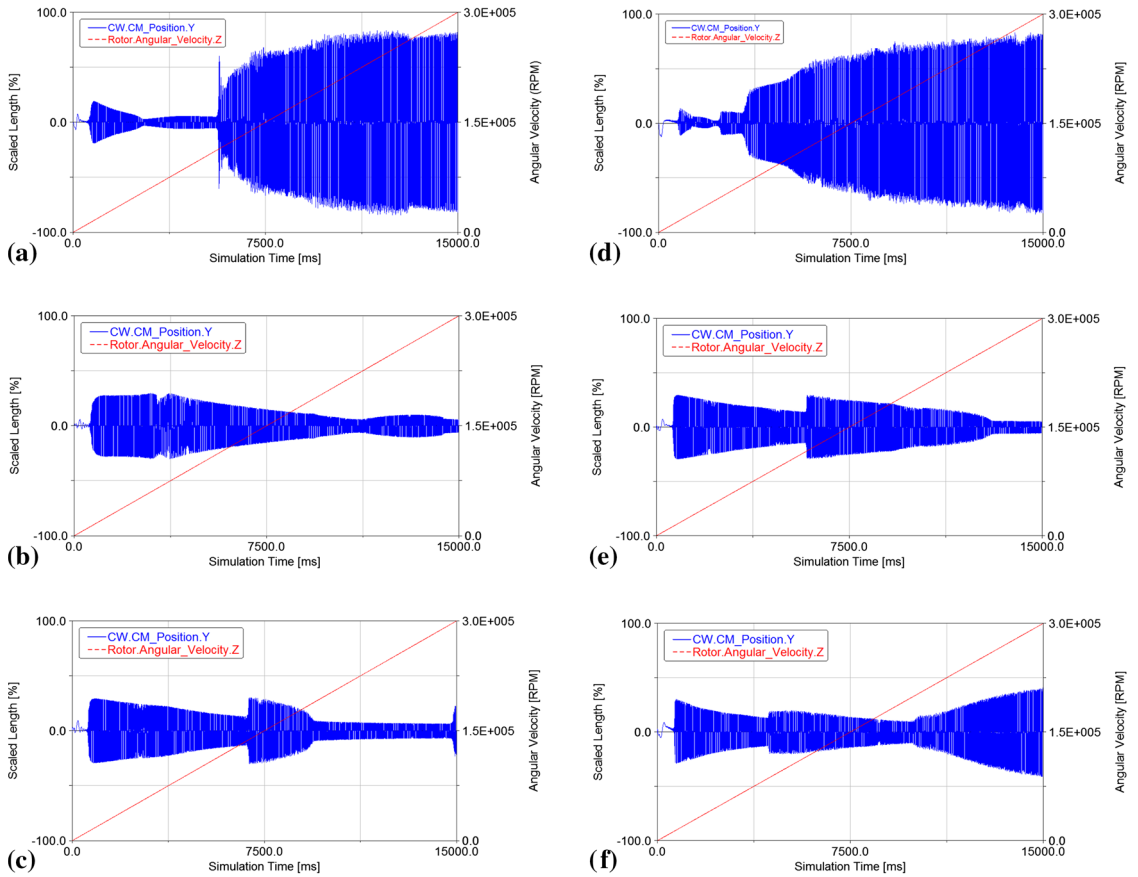

Fig. 10 Comparison of compressor wheel's center of mass radial displacement: Reference **a**, **d**—best **b**, **e**–compromise **b**, **e**; **a** through **c** with $T_{\text{sup}} = 90\,^{\circ}\text{C}$ and **d** through **f** with $T_{\text{sup}} = 150\,^{\circ}\text{C}$

clearance range (feasible construction w.r.t. to cost and robustness). Under consideration of the aforesaid, the results (reference, best and compromise case) are gathered in Table 8 and are compared in form of the compressor wheel's radial displacement, eccentricities and waterfall diagrams depicted in Figs. 10, 11 and 12, respectively.

As observed in Figs. 10, 11 and 12, in the reference configuration, the outer oil-film of both bearings destabilizes at a small RPM threshold ending with high radial displacement responses, whereas the best case offers an overall Sub_3-stability throughout the whole RPM range for both $T_{\text{sup}} = 90\,^{\circ}\text{C}$ and $T_{\text{sup}} = 150\,^{\circ}\text{C}$. Nevertheless, the best-case scenario suffers from extended constant tone problems (Sub_2), when $T_{\text{sup}} = 150\,^{\circ}\text{C}$. The compromised design delivers a well-stabilized rotor for the cold oil supply conditions, but ends up with Sub_3 response at the end of the RPM range.

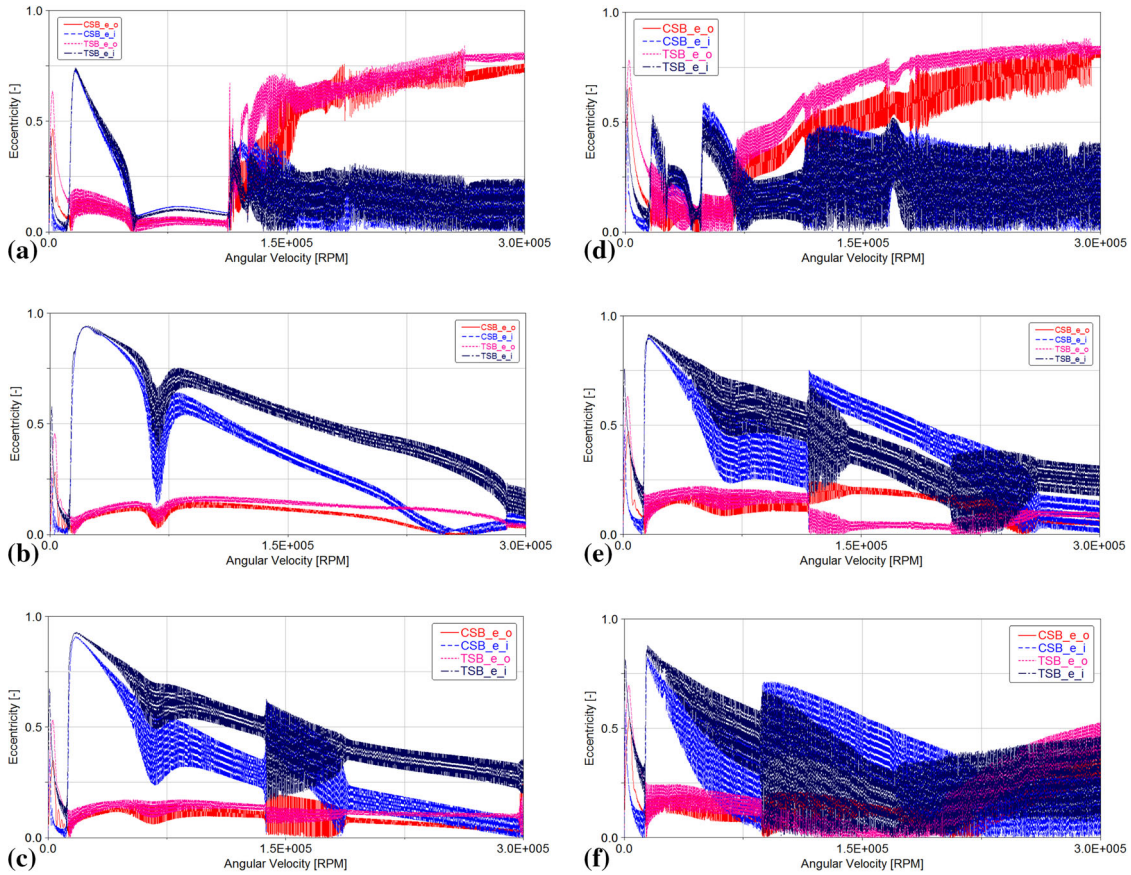

Fig. 11 Comparison inner & outer bearing eccentricities: Reference **a**, **d**—best **b**, **e**—compromise **b**, **e**; **a** through **c** with $T_{\text{sup}} = 90\,^{\circ}\text{C}$ and **d** through **f** with $T_{\text{sup}} = 150\,^{\circ}\text{C}$

6 Conclusions

In this paper, a methodology is applied for the case of a turbocharger rotor with full-floating ring bearings that allows the quantification of the sub-synchronous vibrations during run-up simulations. It is conducted by considering both the wheel shaft, i.e., macro-geometry, and shaft-bearing geometry, i.e., micro-geometry, as a set of input parameters, the variation of which contributes in quantifying their influence upon the sub-synchronous evolution with respect to amplitude and duration criteria.

In contrast to the current standards, a different approach is undertaken in an effort to account for both qualitative as well as quantitative information w.r.t. the influence of the investigated parameters on specified system responses, but also among the responses themselves. In this regard, a configuration response space with 13 quantities (Table 1) has been defined aiming at capturing in detail all possible rotor dynamic effects during a run-up simulation, e.g., which the oil-film destabilizes, the sub-synchronous amplitudes along with the associated duration.

Motivated by linear multivariate regression algorithms and data mining techniques, i.e., correlation coefficients and global sensitivity methods, the influence of each design parameter on the sub-synchronous formation is analyzed and more importantly quantified.

The macro-geometry results impose the shaft diameter D (Fig. 3) being the most influential input variable (39 % influence) upon the global set of responses. On the other hand, the role of L_{TB} is subordinate (10 % influence), whereas L_{CB} and L_B are rated as equally important (26 and 25 % influence, respectively). The latter though exhibit controversial properties w.r.t. the amplitude of Sub_3 and the CSB and TSB outer oil-film. Therefore, L_B and L_{CB} should be designed so as to neutralize the inherited opposite effects between the CSB and TSB oil-films, and Sub_3 itself. In this regard, an optimum macro-geometry design is proposed (Table 6).

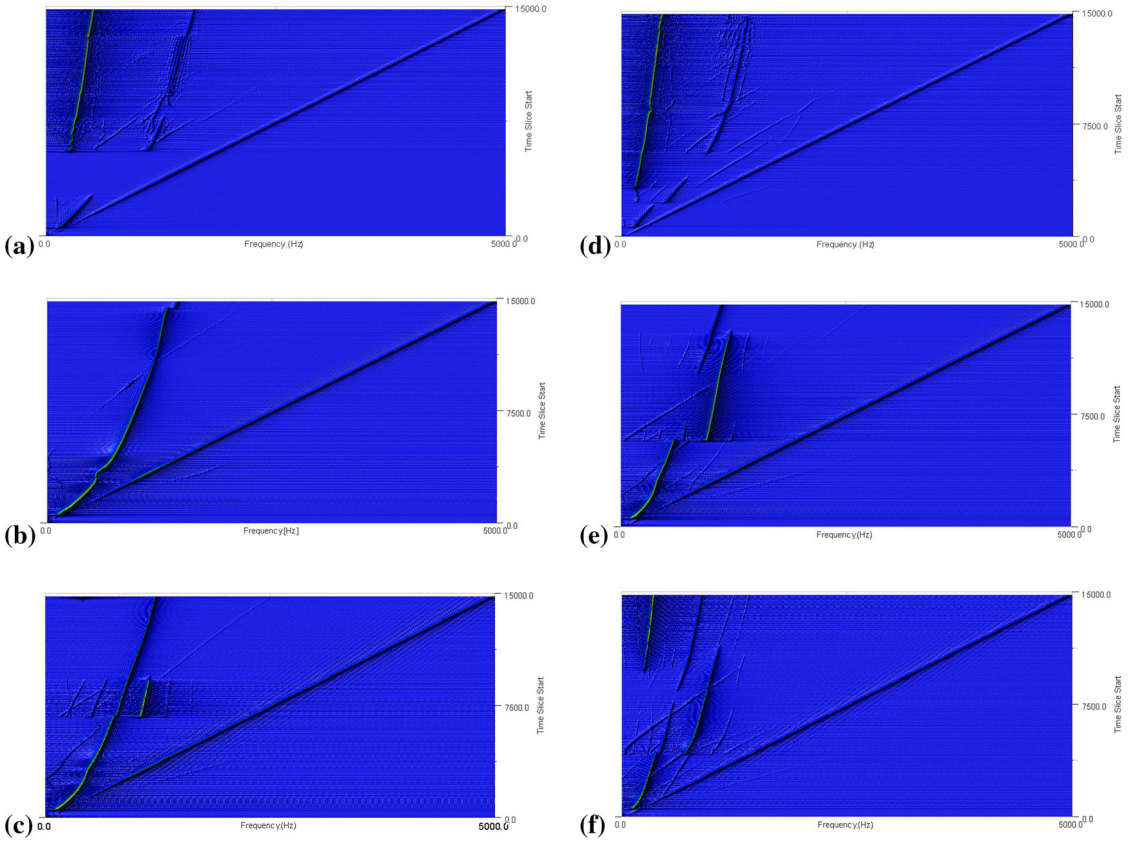

Fig. 12 Comparison waterfall diagram: Reference **a**, **d**—best **b**, **e**—compromise **b**, **e**; **a** through **c** with $T_{\text{sup}} = 90\,^{\circ}\text{C}$ and **d** through **f** with $T_{\text{sup}} = 150\,^{\circ}\text{C}$

The micro-geometry results show that almost 40 % of the system's global response (Table 1) is controlled by the design of the outer clearances (CSB_{ψ_o} & TSB_{ψ_o}), thus directly indicating the compulsory design modification. The bearings' outer width is further listed as important factor, which along with the outer clearances contribute in influencing over 55 % of the system's global response. An enlargement of the bearing outer width although Sub_3-beneficial, it acts contra-productive w.r.t. to constant tone problems (Sub_2). Additionally, the oil supply temperature is ranked as the fourth most important parameter, thus directly affecting the associated bearing speed.

Since, a turbocharger rotor has to perform equally well under cold and warm conditions (cold-start or friction loss problems), the presented results are extended by applying the Self-Organizing Maps methodology in order to account for a feasible rotor assembly design that would hold on to the addressed cold and warm prerequisites. On that basis, a best and a compromise rotor assembly configuration is proposed (Table 8), the results of which are illustrated using the classic rotor dynamics outputs (Figs. 10, 11, 12).

The aforementioned results are to be taken as a specific solution w.r.t. the sub-synchronous problems in case of small-sized high-speed rotors with full-floating ring bearings. Different configurations of small-sized or larger sized rotors with either semi- or full-floating ring bearings do not necessarily hold on to the current proposed design modifications, but the proposed methodology could be applied in order to derive and quantify the most influential parameters and suggest a modified rotor assembly design.

Appendix A: Hydrodynamic bearing model

In this section, the hydrodynamic bearing model used throughout the simulations of the current paper is briefly explained. Figure 13 depicts the sectional drawing of a plain circular hydrodynamic bearing, based on which the derivation of the two-dimensional Reynolds equation [14,26,35,39] is formulated as given in (8), i.e.,

$$\frac{\partial}{\partial x}\left[h^3\frac{\partial p}{\partial x}\right]+\frac{\partial}{\partial z}\left[h^3\frac{\partial p}{\partial z}\right]=6\mu\left[U\frac{\partial h}{\partial x}+2\frac{\partial h}{\partial t}\right]. \tag{8}$$

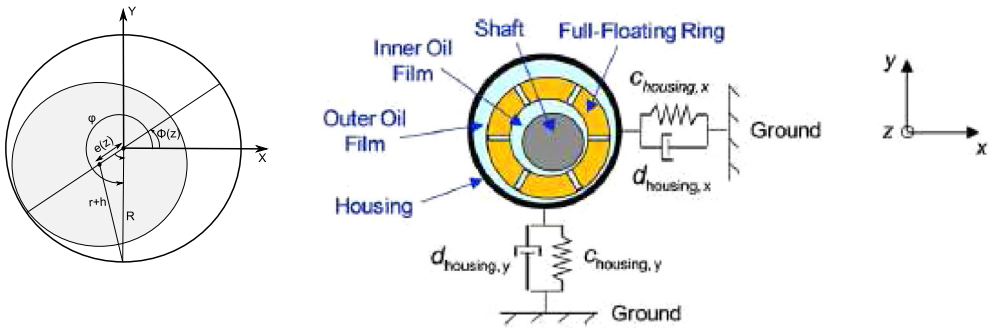

Fig. 13 *Left-hand side* display of oil-film thickness & *right-hand side* cross section through full-floating ring bearing:elastically bedded housing, ring and shaft as given in [33]

Here, p represents the oil-film pressure, μ the dynamic oil viscosity and U is the circumferential velocity component of the associated valve guide, which due to the presence of viscosity coincides to the associated velocity component of the fluid. Thus, for the inner oil-film, the velocity component of the shaft coincides with the velocity component of the inner oil-film, and for the outer oil-film, the velocity component of the bearing coincides with the associated velocity component of the outer oil-film. The term $h := h(x, z)$ refers to the oil-film thickness (Fig. 13), which described in cylindrical coordinates equals to $h = R - r + e(z)\cos(\varphi - \phi(z))$.

Equation (8) is solved for both the inner and the outer oil-film and the associated oil-film pressure p is obtained. Thereafter, the friction torque M_{R} is calculated by integrating the shear stress over the bearing surface [26,35], i.e.,

$$M_{\mathrm{R}} = R \int_z \int_x \boldsymbol{\tau} \mathrm{d}x\mathrm{d}z, \quad \text{with} \quad \boldsymbol{\tau} = \mu \frac{\partial u}{\partial y} = \frac{1}{2}\frac{\partial p}{\partial x} h + \mu \frac{U}{h} \tag{9}$$

The overall hydrodynamic bearing force is calculated by the double integral of the resultant pressure distribution $F_{\mathrm{B}} = \int_z \int_x P \mathrm{d}x\mathrm{d}z$ (for both the inner and the outer oil-film [35], but without accounting for oil-flow interaction between the two films).

The aforementioned solution procedure is integrated into (3)–(6), i.e., the information w.r.t. bearing eccentricities and the associated oil-film thickness along with the associated time derivatives are used as input for solving (8). Thereafter, the resulting bearing forces and friction torques are used in (3)–(6) for computing the multi-body dynamics.

Appendix B: Study I

Appendix B.1: Study I: Coefficient of importance—CoI

The coefficient of importance (CoI) indicates the possible multivariate dependencies of a group of input parameters and explains the influence of a single explanatory variable $\mathbf{x}_s$ among the complete set of input variables on a chosen response.

Let $\mathbf{X}^{n\times v} = [\mathbf{x}_1\ \mathbf{x}_2\ \ldots\ \mathbf{x}_s\ \ldots\ \mathbf{x}_v]$ be the matrix of all v explanatory variables and $\mathbf{Y}^{n\times r} = \left[\mathbf{y}_1\ \mathbf{y}_2\ \ldots\ \mathbf{y}_r\right]$ the associated matrix of r responses. Here, n denotes the total number of configurations and s corresponds to a random explanatory variable, which is utilized for calculating the CoI as follows, i.e.,

$$\mathrm{CoI}_{j,s} = R_j^2 - R_{j,s}^2, \quad j = 1, 2, \ldots, r \tag{10}$$

$$R_j = \frac{\left\| \hat{\mathbf{y}}_j(\mathbf{x}_1, \mathbf{x}_2, \ldots, \mathbf{x}_s, \ldots, \mathbf{x}_v) - \bar{\hat{\mathbf{y}}}_j \right\|^2}{\left\| \mathbf{y}_j(\mathbf{x}_1, \mathbf{x}_2, \ldots, \mathbf{x}_s, \ldots, \mathbf{x}_v) - \bar{\mathbf{y}}_j \right\|^2} \tag{11}$$

$$R_{j,s} = \frac{\left\| \hat{\mathbf{y}}_{j,s}(\mathbf{x}_1, \mathbf{x}_2, \ldots, \mathbf{x}_{s-1}, \mathbf{x}_{s+1}, \ldots, \mathbf{x}_v) - \bar{\hat{\mathbf{y}}}_j \right\|^2}{\left\| \mathbf{y}_j(\mathbf{x}_1, \mathbf{x}_2, \ldots, \mathbf{x}_{s-1}, \mathbf{x}_{s+1}, \ldots, \mathbf{x}_v) - \bar{\mathbf{y}}_j \right\|^2} \tag{12}$$

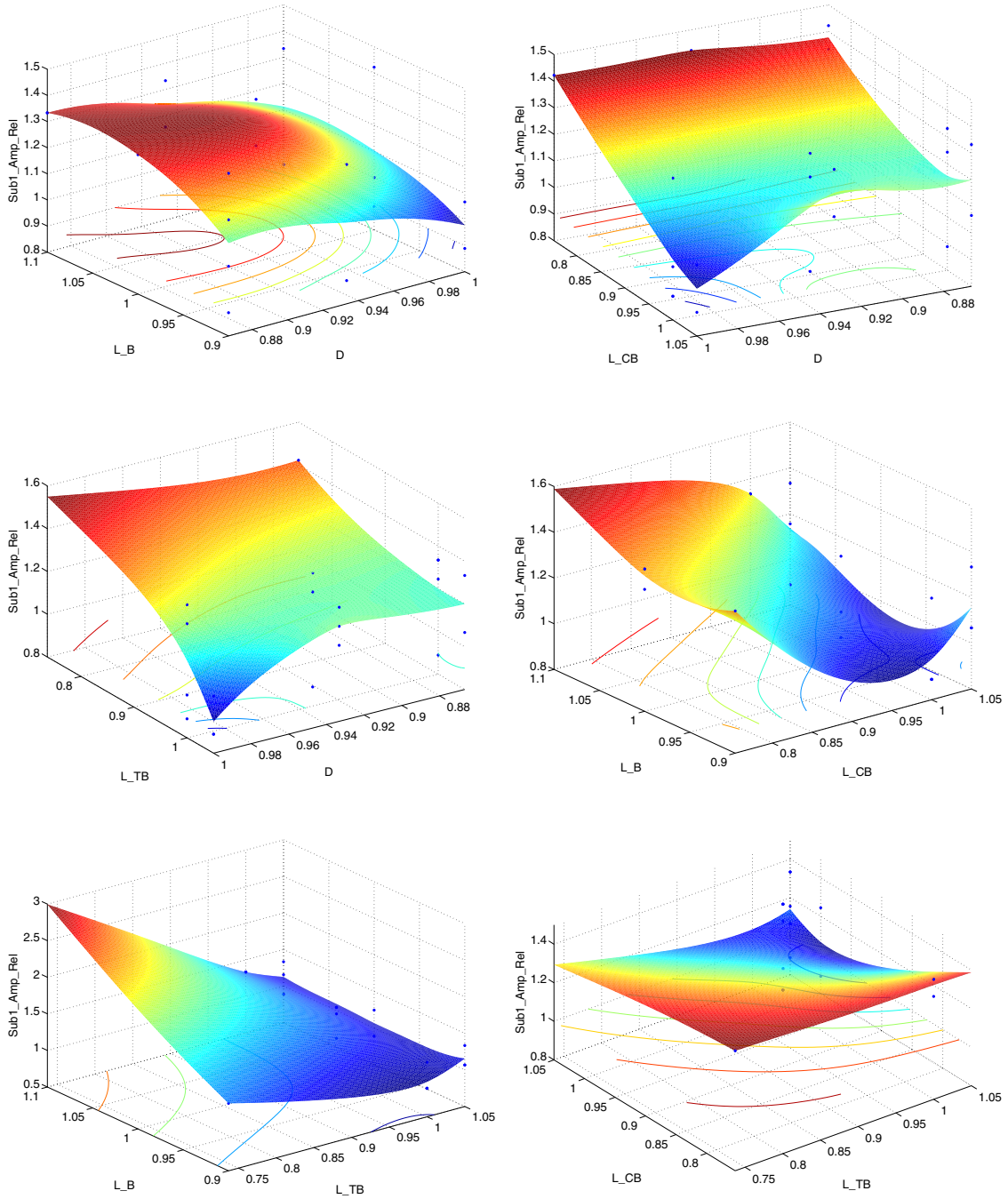

Fig. 14 Study I—response surface for $\text{Sub}_1^{\text{amp}}$—normalized data

with $\text{CoI}_{j,s}$ denoting the CoI of the explanatory variable $\mathbf{x}_s$ on the selected response $\mathbf{y}_j$. The terms $\hat{\mathbf{y}}_j$ and $\hat{\mathbf{y}}_{j,s}$ refer to the regression fitted values by including and excluding $\mathbf{x}_s$, respectively. The CoI calculation of all explanatory variables leads to the definition of the associated $\text{CoI}^{r\times v}$ matrix, which can be written as

$$\mathbf{CoI} = \begin{bmatrix} \text{CoI}_{1,1} & \text{CoI}_{1,2} & \dots & \text{CoI}_{1,v} \\ \text{CoI}_{2,1} & \text{CoI}_{2,2} & \dots & \text{CoI}_{2,v} \\ \vdots & \vdots & \vdots & \vdots \\ \text{CoI}_{r,1} & \text{CoI}_{r,2} & \dots & \text{CoI}_{r,v} \end{bmatrix}. \tag{13}$$

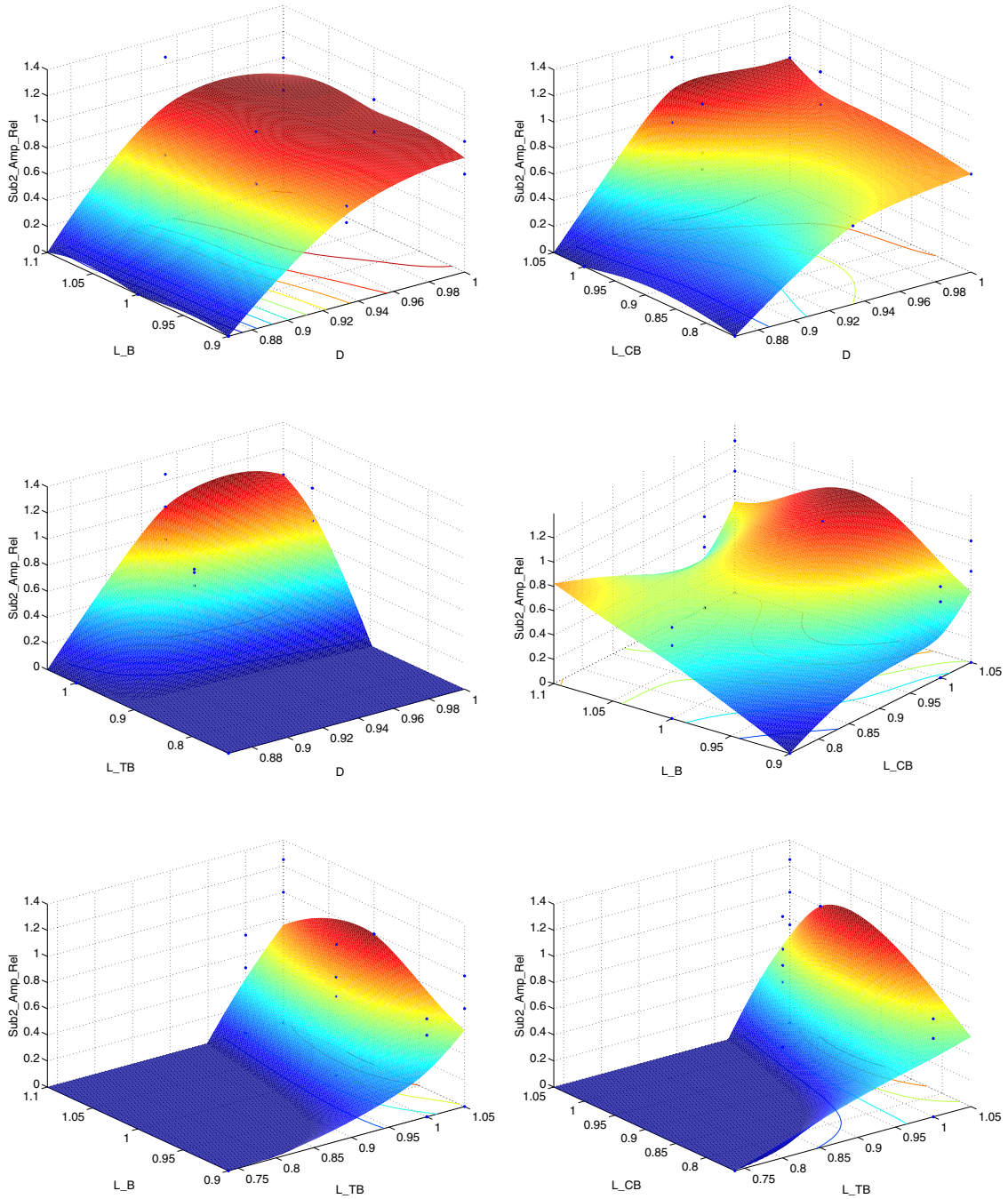

Fig. 15 Study I—response Surface for Sub_2^{amp}—normalized data

Appendix B.2: Study I: Response surface methodology—RSM

Here, the RSM algorithms are applied, which are defined in [12,32]. The purpose of utilizing a RSM process is to enable the evolution of the compared data, which go beyond the boundaries or cover as different points defined in the associated variational study.

The RSM data depicted in Fig. 14, 15 and 16 serve the purpose of establishing the proposed macro design parameters in Table 6 as being the optimum design. All possible parameter combinations are given for each sub-synchronous response (all parameters vs. Sub_1^{amp} in Fig. 14, vs. Sub_2^{amp} in Fig. 15 and vs. Sub_3^{amp} in Fig. 16) thus, capturing their combined effect upon the associated response.

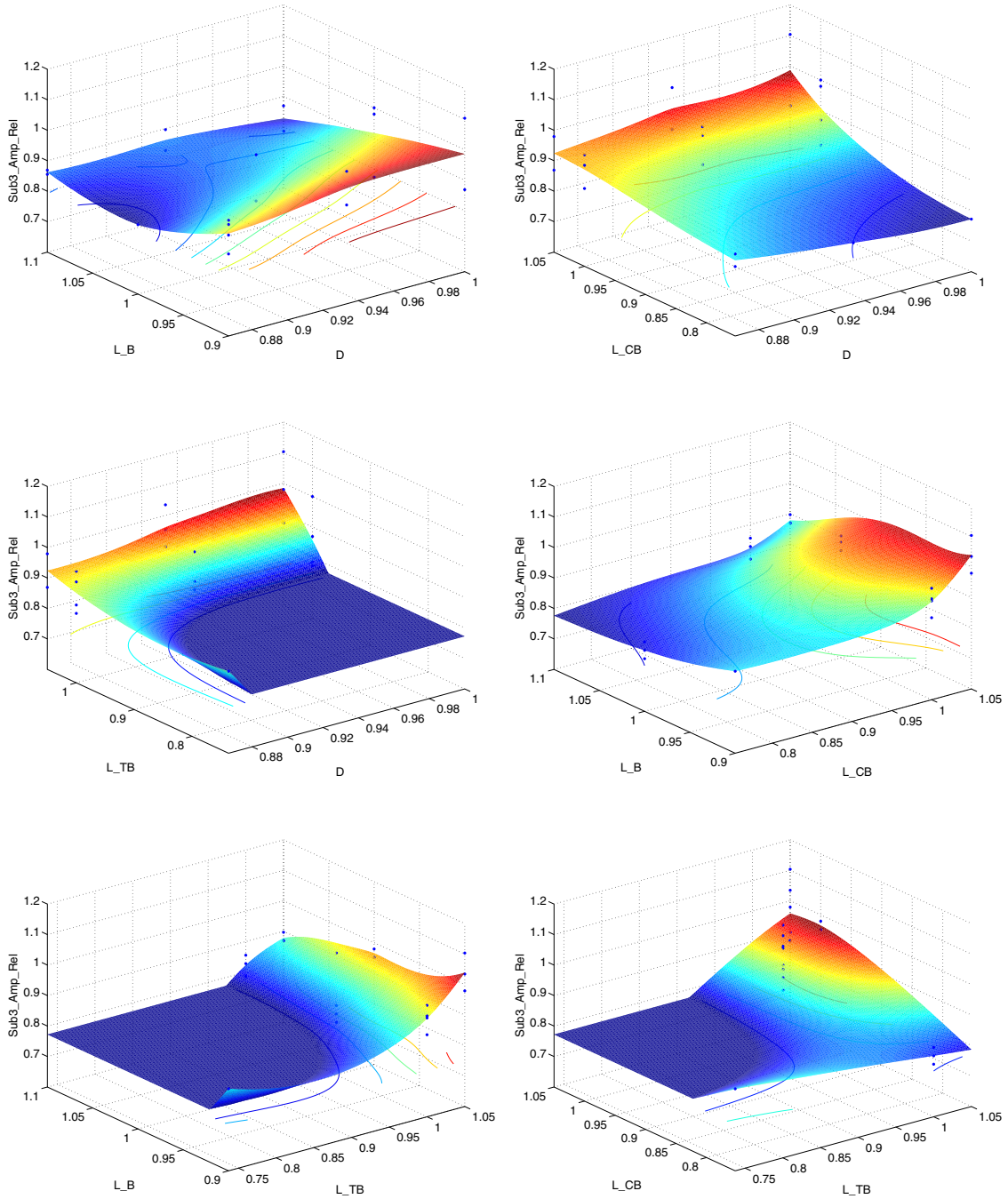

Fig. 16 Study I—response Surface for $\mathrm{Sub}_3^{\mathrm{amp}}$—normalized data

Appendix B.3: Study I: Sensitivity analysis—individual responses

Figure 17 collects the information w.r.t. the parameter influence upon each individual response, while taking into consideration the whole set of responses. The sum of the absolute percentage variation values equals 100 % thus, indicating both the amount as well as the positive or negative parameter influence on the evolution of the associated response.

The sensitivity analysis results for individual responses, e.g., as depicted in Fig. 17 can be effectively utilized in order to capture the impact of a design modification on a specific response. Nevertheless, these

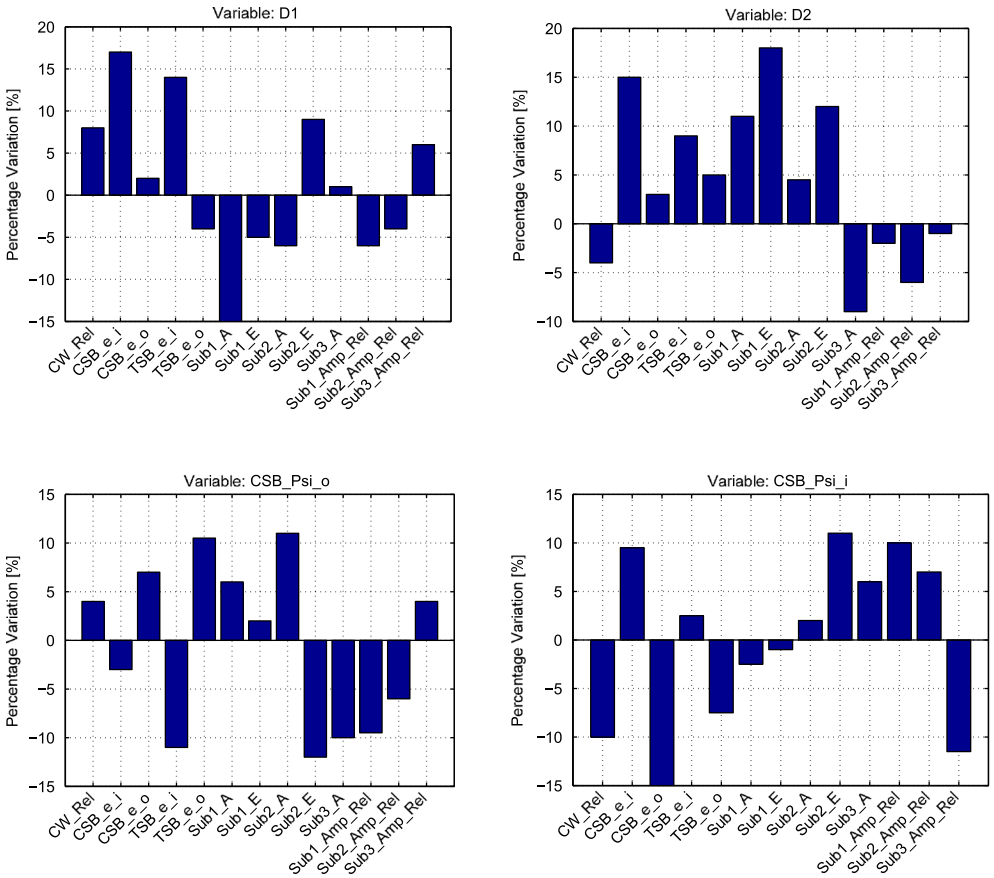

Fig. 17 Study I: Sensitivity analysis on individual responses

data should serve as supplementary information to the results gathered in Table 5 and Figs. 5, 6, since dynamic responses cannot be isolated from each other and the global system response is ultimately important.

Appendix C: Study II

Appendix C.1: Study II: Sensitivity analysis—individual responses

For a short description on how Figs. 18 and 19 should be read, see B.3. Figures 18, 18 and 19 serve as supplementary information to the results gathered in Table 7 and Fig. 8.

Appendix C.2: Study II: Self-organizing map (SOM)

The self-organizing map (SOM) methodology is applied [20,21] using the SOM MATLAB toolbox [41]. For the purpose of the current study the sequential training algorithm has been applied, which is briefly outlined in the following (in the exact way as described in [26]). For an in-depth description of the method see [20,21,41].

Assume the high-dimensional input data (variables and responses in Sect. 3) be represented by a d-dimensional set of vectors. A weight vector $M = [m_1 \quad m_2 \quad \dots \quad m_d]^T \in \mathbb{R}^d$ is associated with each element of the SOM array, which additionally is of equal dimension. At each training step, a random sample vector $\mathbf{x}$ is selected from the input set and the associated distances w.r.t. to the weight vectors are calculated. Herewith, the best-matching unit (BMU) is ascertained [20], which is calculated by allocating the node index c with the minimum distance—Euclidean distance—from the input vector [41]:

$$\|\mathbf{x} - \mathbf{m}_c\| = \min_i \{\|\mathbf{x} - \mathbf{m}_i\|\} \tag{14}$$

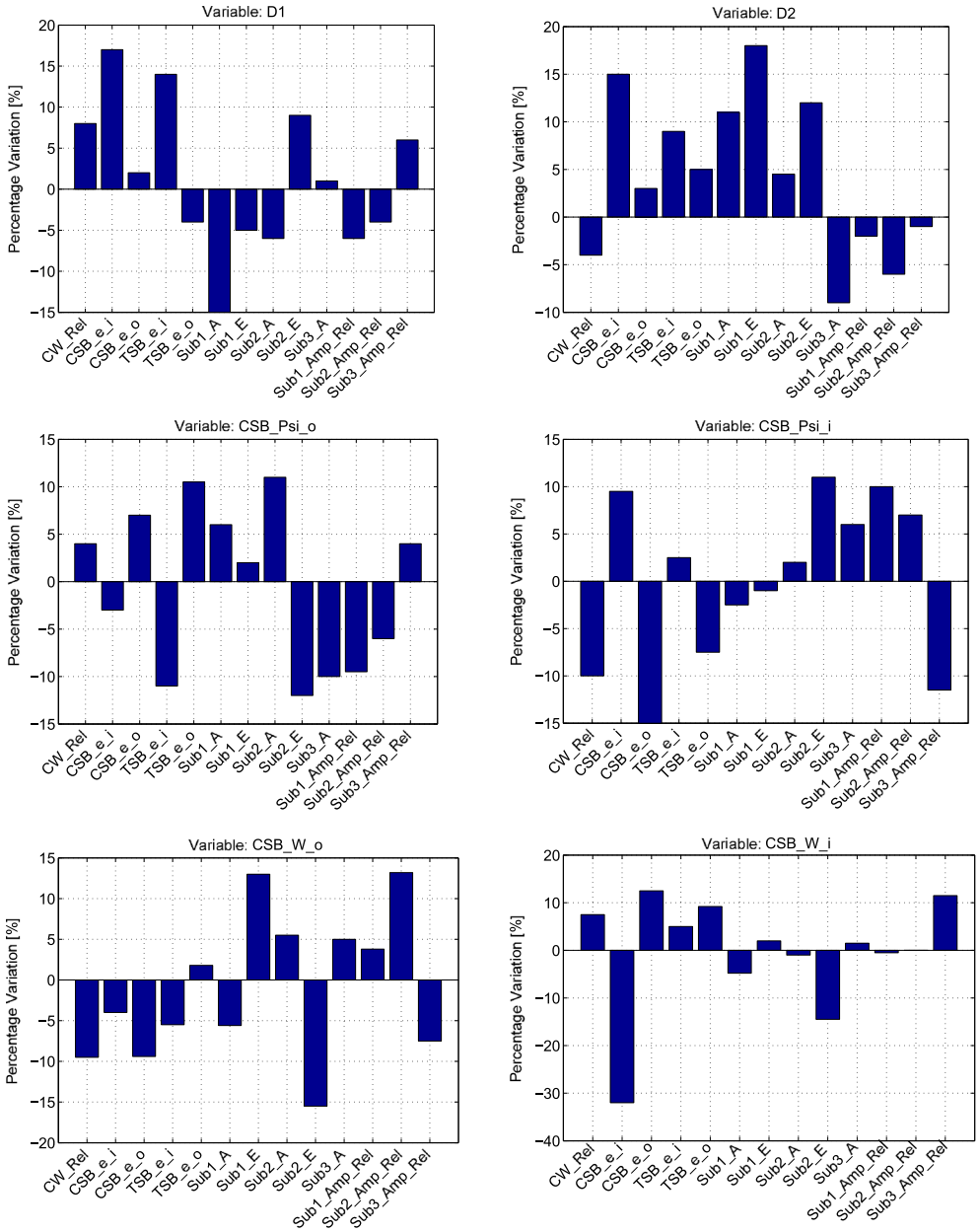

Fig. 18 Study II: Sensitivity on individual responses I

The SOM weight vectors $\mathbf{m}_i$ are updated such that BMU gradually approaches the input vector in the input space with the associated BMU topological neighbors conducting the same procedure. The time-dependent update algorithm used therefore is [20,21,41]:

$$\mathbf{m}_i(t+1) = \mathbf{m}_i(t) + \alpha(t) h_{ci}(t) \left[\mathbf{x}(t) - \mathbf{m}_i(t)\right], \tag{15}$$

with $\alpha(t)$ being the monotonically decreasing learning rate [20,21,41], $h_{ci}(t)$ the neighborhood function around the computed unit c and t the time. A random initialization scheme is chosen for the SOM generation and the Gaussian function is used for allocating the neighborhood function $h_{ci}(t)$ as defined in [41], i.e.,

$$\begin{aligned} h_{ci}(t) &= e^{-d_{ci}^2/2\sigma_t^2} \\ \sigma_t &: \text{ neighborhood radius at time } t \\ d_{ci} &: \text{ distance between the map units } c \text{ and } i \text{ on the map grid} \end{aligned} \tag{16}$$

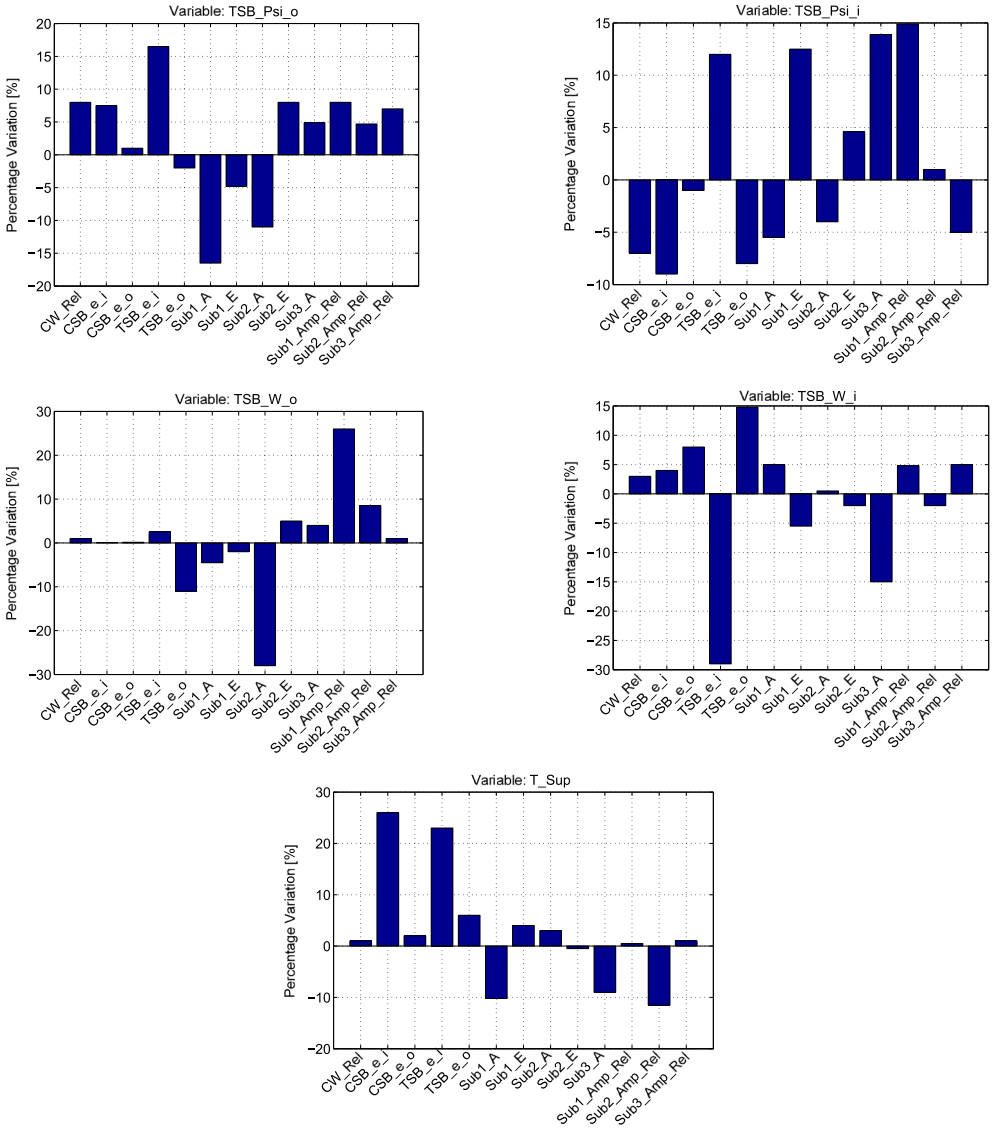

Fig. 19 Study II: Sensitivity on individual responses II

References

1. Arnold, M., Burgermeister, B., Führer, C., Hippmann, G., Rill, G.: Numerical methods in vehicle system dynamics: State of the art and current developments. Veh. Syst. Dyn. **49**, 1159–1207 (2011)
2. Arnold, M., Burgermeister, B., Führer, C., Hippmann, G., Rill, G.: Simulation algorithms and software tools. In: G. Mastinu, M. Plöchl (eds.) Road and Off-Road Vehicle System Dynamics Handbook, pp. 45–68, CRC Press (2014)
3. Boyaci, A.: Zum Stabilitäts- und Bifurkationsverhalten hochtouriger Rotoren in Gleitlagern. Ph.D. thesis, Karlsruher Institut für Technologie (2012)
4. Boyaci, A., Backhaus, K., Koch, R.: Hochlaufsimulation: Mehrkörpersimulation des Hochlaufverhaltens von ATL-Rotoren mit nichtlinear modellierten Schwimmbuchsenlagern. Tech. Rep. 889, FVV e. V. (2009)
5. Brenan, K.E., Campbell, S.L., Petzold, L.R.: Numerical solution of initial-value problems in differential-algebraic equations. Classics in Applied Mathematics. SIAM—Society for Industrial and Applied Mathematics, Philadelphia (1996)
6. Butenschön, H.J.: Das hydrodynamische, zylindrische Gleitlager endlicher Breite unter instationärer Belastungen. Ph.D. thesis, TH Karlsruhe (1976)
7. Craig, Jr. R.R.: Coupling of substructures for dynamic analyses: an overview. AIAA-2000-1573 (2000)
8. Craig, R., Bampton, M.: Coupling of substructures in dynamic analysis. AIAA **6** (1968)
9. Driot, N., Berlioz, A., Lamarque, C.-H.: Stability and stationary response of a skew Jeffcott rotor with geometric uncertainty. J. Comput. Nonlinear Dyn. **4**(2):02100302100310 (2009)

10. Driot, N., Lamarque, C.-H, Berlioz, A.: Theoretical and experimental analysis of a base-excited rotor. J. Comput. Nonlinear Dynam. **1**(3) (2006)
11. Duchemin, M., Berlioz, A., Ferraris, G.: Dynamic behavior and stability of a rotor under base excitation. J. Vib. Acoust. **128**(5), 576–585 (2006)
12. DYNARDO GmbH: optiSLang-the optimizing Structural Language: Sensitivity analysis, multidisciplinary optimization, robustness evaluation, reliability analysis and robust design optimization, 3.2.1 edn (2011)
13. Garcíade Jalón, J., Gutiérrez-López, M.D.: Multibody dynamics with redundant constraints and singular mass matrix: existence, uniqueness, and determination of solutions for accelerations and constraint forces. Multibody Syst. Dyn. **30**, 311–341 (2013)
14. Gasch, R., Nordmann, R., Pfützner, H.: Rotordynamik. 2nd edn. Springer, Berlin (2001)
15. Gear, C.W., Leimkuhler, B., Gupta, G.K.: Automatic integration of Euler–Lagrange equations with constraints. J. Comput. Appl. Math. **12**, 77–90 (1985)
16. Golub, G.H., Van Loan, C.F.: Matrix Computations. The John Hopkins University Press, Baltimore, MD (1996)
17. Hammersley, J.M., Handscomb, D.C.: Monte Carlo Methods. Chapman & Hall, London (1964)
18. Holt, C., San Andrés, L., Sahay, S., Tang, P., LaRue, G., Gjika, K.: Test response of a turbocharger supported on floating ring bearings Part I: Assessment of subsynchronous motions. In: 19th Biennial Conference on Mechanical Vibration and Noise (2003)
19. Jobson, J.D. : Applied Multivariate Data Analysis: Regression and Experimental Design. Springer, Berlin (1999)
20. Kohonen, T.: The self-organizing map. Proc. IEEE **78**, 1464–1480 (1990)
21. Kohonen, T.: Self-organizing maps. In: Information Sciences, Vol. **30**, 2 edn. Springer, Berlin (1997)
22. Koutsovasilis, P.: Model order reduction in structural mechanics: coupling the rigid and elastic multi body dynamics. Ph.D. thesis, Technische Universität Dresden (2009)
23. Koutsovasilis, P.: Improved component mode synthesis and variants. Multibody Syst. Dyn. **29**, 343–359 (2013)
24. Koutsovasilis, P., Beitelschmidt, M.: Simulation of constrained mechanical systems. In: PAMM Proc. Appl. Math. Mech., vol. **7**, pp. 4010041–4010042 (2007)
25. Koutsovasilis, P., Beitelschmidt, M.: Model order reduction of finite element models: improved component mode synthesis. Math. Comput. Model. Dyn. Syst. **16**(1), 57–73 (2010)
26. Koutsovasilis, P., Schweizer, B.: Parameter variation and data mining of oil film bearings—a stochastic study on the Reynolds equation of lubrication. Arch. Appl. Mech. **80**(9), 1017–1043 (2014)
27. Montgomery, D.C. : Design and Analysis of Experiments. Wiley, NY (2005)
28. Montgomery, D.C., Myers, R.H.: Response surface methodology: process and product in optimization using designed experiments. Wiley, NY (1995)
29. Nguyen-Schäfer, H.: Rotordynamics of automotive turbochargers: linear and nonlinear rotordynamics—bearing design—rotor balancing. Springer, Berlin Heidelberg (2012)
30. San Andrés, L., Rivadeneira, J.C., Chinta, M., Gjika, K., LaRue, G.: Nonlinear rotordynamics of automotive turbochargers predictions and comparisons to test data. ASME J. Eng. Gas Turbines Power **129**, 488–493 (2007)
31. San Andrés, L., Vistamehr, A.: Nonlinear rotordynamics of vehicle turbochargers: parameters affecting sub harmonic whirl frequencies and their jump. In: 8th IFToMM International Conference on Rotordynamics (2010)
32. Sathyanarayana K.K.: MATLAB GUI Implementierung—Statistik & Data Mining. Studienarbeit, Institut für Wissenschaftliches Rechnen, Technische Universität Braunschweig (2013)
33. Schweizer, B.: Total instability of turbocharger rotors-physical explanation of the dynamic failure of rotors with full-floating ring bearings. J Sound Vib **328**, 156–190 (2009)
34. Schweizer, B.: Vibrations and bifurcations of turbocharger rotors. In: SIRM 2009—8th International Conference on Vibrations in Rotating Machines (2009)
35. Schweizer, B.: Dynamics and stability of automotive turbochargers. Arch. Appl. Mech. **80**(9), 1017–1043 (2010)
36. Schweizer, B., Sievert, M.: Nonlinear oscillations of automotive turbocharger turbines. J. Sound Vib. **321**, 955975 (2009)
37. Schwertassek, R., Wallrapp, O.: Dynamik flexibler Mehrkörpersysteme: Methoden der Mechanik zum rechnergestützten Entwurf und zur Analyse mechatronischer Systeme. Vieweg (1999)
38. Shabana, A.A.: Dynamics of Multibody Systems. Cambridge University Press, University of Illinois at Chicago, Chicago (2005)
39. Szeri, A.Z.: Fluid Film Lubrication: Theory and Design. Cambridge University Press, Cambridge (2005)
40. Vance, J.M.: Rotordynamics of Turbomachinery. Wiley, New York (1988)
41. Vesanto, J., Alhoniemi, E., Himberg, J., Kiviluoto, K., Parhankangas, J.: Self-organizing map for data mining in MATLAB: the SOM toolbox. Simul. News Eur. **25**(54) (1999)